Journal of Magnetic Resonance 212 (2011) 154–160

Contents lists available at ScienceDirect

Journal of Magnetic Resonance

journal homepage: www.elsevier.com/locate/jmr

# Avoiding eddy-current problems in ultra-low-field MRI with self-shielded polarizing coils

Jaakko O. Nieminen [a,*], Panu T. Vesanen [a], Koos C.J. Zevenhoven [a], Juhani Dabek [a], Juha Hassel [b], Juho Luomahaara [b], Jari S. Penttilä [c], Risto J. Ilmoniemi [a]

[a] Department of Biomedical Engineering and Computational Science, Aalto University School of Science, P.O. Box 12200, FI-00076 AALTO, Finland
[b] VTT Technical Research Centre of Finland, P.O. Box 1000, FI-02044 VTT, Finland
[c] Aivon Oy, Tietotie 3, FI-02150 Espoo, Finland

ARTICLE INFO

*Article history:*
Received 28 April 2011
Revised 10 June 2011
Available online 1 July 2011

*Keywords:*
Polarizing coil
Ultra-low-field MRI
Eddy currents
Magnetically shielded room
Multipole expansion

ABSTRACT

In ultra-low-field magnetic resonance imaging (ULF MRI), superconductive sensors are used to detect MRI signals typically in fields on the order of 10–100 μT. Despite the highly sensitive detectors, it is necessary to prepolarize the sample in a stronger magnetic field on the order of 10–100 mT, which has to be switched off rapidly in a few milliseconds before signal acquisition. In addition, external magnetic interference is commonly reduced by situating the ULF-MRI system inside a magnetically shielded room (MSR). With typical dipolar polarizing coil designs, the stray field induces strong eddy currents in the conductive layers of the MSR. These eddy currents cause significant secondary magnetic fields that may distort the spin dynamics of the sample, exceed the dynamic range of the sensors, and prevent simultaneous magnetoencephalography and MRI acquisitions. In this paper, we describe a method to design self-shielded polarizing coils for ULF MRI. The experimental results show that with a simple self-shielded polarizing coil, the magnetic fields caused by the eddy currents are largely reduced. With the presented shielding technique, ULF-MRI devices can utilize stronger and spatially broader polarizing fields than achievable with unshielded polarizing coils.



## 1. Introduction

In ultra-low-field magnetic resonance imaging (ULF MRI), MR images are acquired in fields on the order of 10–100 μT [1,2]. Because the precession frequencies are low, it is preferable to measure the signals using very low-noise detectors, *e.g.*, superconducting quantum interference device (SQUID) sensors [1], atomic magnetometers [3], or giant magnetoresistance (GMR) sensors [4,5]. The use of highly sensitive SQUID sensors with low $1/f$ noise allows one to combine MRI with magnetoencephalography (MEG) [6,7].

Despite the highly sensitive detectors, it is necessary to prepolarize the sample in a magnetic field $\boldsymbol{B}_\mathrm{p}$ on the order of 10–100 mT before signal encoding and acquisition occurs in a weak homogeneous field $\boldsymbol{B}_0$ and gradient fields. When the signal is measured with an untuned SQUID sensor, its amplitude is independent of the signal frequency, and thus also of $B_0$, and proportional to $B_\mathrm{p}$. In ULF MRI, image signal-to-noise ratio (SNR) is a limiting factor; thus, the imaging time for a given spatial resolution (voxel volume) depends on SNR as $1/\mathrm{SNR}^2 \propto (B_\mathrm{N}/B_\mathrm{p})^2$, where $B_\mathrm{N}$ is the noise amplitude. Therefore, the polarizing field should be as high and the noise level as low as possible to obtain high-quality images in a short imaging time.

Typically, $B_\mathrm{N}$ is reduced by providing shielding against external noise sources. For ULF MRI at the kilohertz range, a light magnetically shielded room (MSR) of an aluminum layer around the measurement system together with gradiometric sensors are enough to render the external noise insignificant [8]. If ULF MRI is combined with MEG, additional shielding at lower frequencies is usually needed. Such a shielding can be achieved with an MSR consisting of a few layers of $\mu$-metal with high permeability, together with thicker layers of aluminum [9].

However, combining the shielding and high polarizing fields is problematic. Because the polarizing field has to be switched off in a few milliseconds, a large time-derivative $\partial\boldsymbol{B}_\mathrm{p}/\partial t$ appears. With dipolar polarizing coil designs presented in literature [8,10,11], an extended stray field (or fringe field) occurs with $\boldsymbol{B}_\mathrm{p}$. Thus, when a typical polarizing field is switched off, strong eddy currents are induced in the conductive layers of the MSR [12,13]. These currents decay in a multi-exponential manner depending on the resistances and inductances of the conductive paths. The eddy currents cause secondary magnetic fields inside the MSR. If these fields are strong, they will affect the spin dynamics of the sample, reducing image quality, or, in the worst case, making image reconstruction practically impossible. A large drifting magnetic field may also exceed

* Corresponding author. Fax: +358 9 470 23182.
*E-mail address:* jaakko.nieminen@aalto.fi (J.O. Nieminen).

1090-7807/$ - see front matter © 2011 Elsevier Inc. All rights reserved.
doi:10.1016/j.jmr.2011.06.022

the dynamic range of the SQUID sensors. In addition, such fields typically contain low-frequency components; thus, they may interfere with MEG recordings, frustrating simultaneous MEG–MRI [7].

In high-field MRI, harmful eddy currents are induced because of the rapid switching of the gradient fields. Naturally, they affect the field homogeneity and stability, producing image artifacts. Together with the high static field, the eddy currents cause also vibration and acoustic noise [14]. Therefore, several methods have been developed to minimize the eddy currents.

One of the most widely used techniques is to design gradient coils with weak stray fields. Such self-shielded gradient coils can be designed numerically [15] or analytically in cylindrical [16,17] and planar [18] geometries utilizing Fourier transform techniques. An equivalent approach can also be applied to designing coils that produce shielded homogeneous fields useful in pulsed-field MRI [19]. Also the multipole expansion of a coil can be applied to obtain a design with a reduced stray field [20,21].

Another possibility is to modify the gradient-field waveforms. In the pre-emphasis methods, the current pulse has typically a multi-exponential overshoot at the beginning and an equivalent undershoot at the end [22–24]. Commonly, an iterative approach is needed to design waveform corrections that minimize the eddy currents.

If the static field is produced by a permanent magnet, gradient switching may induce eddy currents in the magnet. It has been demonstrated that by covering the permanent magnet with highly conductive plates, the eddy current problem will be reduced [25]. In that case, eddy currents are induced in the plates with rapid decay rates permitting signal acquisition shortly after gradient ramping.

When magnetic relaxation or nuclear magnetic resonance experiments are performed inside a magnetically shielded room, the magnetization of the MSR may cause problems. In Refs. [26,27], a tiny solenoid is used to polarize the sample; an equivalent coil, with an opposite field direction, is placed next to the polarizing coil to reduce the stray field and to prevent the magnetization of the MSR walls. However, such a design becomes impractical when the sample volume and the strength of the polarizing field increase.

In this paper, we describe a method to design self-shielded polarizing coils for ULF MRI. The method takes into account that the polarizing field homogeneity requirements within the imaging volume are weak; we concentrate on minimizing the stray field outside the coil using the coil's multipole expansion. The approach can be used to design self-shielded coils with arbitrary geometrical constraints, allowing one to find coils that produce shielding against eddy currents, are easy to manufacture, and meet the geometrical constraints of the ULF-MRI system. The theoretical results are verified with experiments using a polarizing coil with and without shielding.

## 2. Theory

In the following, we derive equations that under given geometrical constraints determine how an axially symmetric polarizing coil can be shielded. The aim here is to design a shielding coil that, when connected in series with the polarizing coil, produces a self-shielded polarizing coil with a weak stray field. In general, the method is not limited to the symmetric case.

In current-free space, when displacement currents can be neglected, the magnetic field $\boldsymbol{B}$ is

$$\boldsymbol{B} = -\mu_0 \nabla V, \tag{1}$$

where $\mu_0$ is the permeability of vacuum and the scalar potential $V$ satisfies Laplace's equation,

$$\nabla^2 V = 0. \tag{2}$$

The solution of Eq. (2) can be found using the spherical harmonics $Y_{lm}$ [28]:

$$V(\boldsymbol{r}) = \sum_{l=0}^{\infty}\sum_{m=-l}^{l} \alpha_{lm}\frac{Y_{lm}(\theta,\phi)}{r^{l+1}} + \sum_{l=0}^{\infty}\sum_{m=-l}^{l}\beta_{lm}Y_{lm}(\theta,\phi)r^{l}, \tag{3}$$

where $(r,\theta,\phi)$ are the spherical coordinates. The first sum with multipole moments $\alpha_{lm}$ defines the potential exterior to any current sources. In contrast, the sum with multipole moments $\beta_{lm}$ gives the potential closer to the origin than the current sources. For a current density $\boldsymbol{J}(\boldsymbol{r})$, the multipole moments are [29,30]

$$\begin{aligned}\alpha_{lm} &= \frac{-1}{(2l+1)(l+1)}\int r^{l}Y^{*}_{lm}(\theta,\phi)\nabla\cdot[\boldsymbol{r}\times\boldsymbol{J}(\boldsymbol{r})]dV \\ &= \frac{-1}{(2l+1)(l+1)}\int \boldsymbol{J}(\boldsymbol{r})\cdot[\boldsymbol{r}\times\nabla Y^{*}_{lm}(\theta,\phi)]r^{l}dV\end{aligned} \tag{4}$$

and

$$\beta_{lm} = \frac{1}{(2l+1)l}\int \boldsymbol{J}(\boldsymbol{r})\cdot[\boldsymbol{r}\times\nabla Y^{*}_{lm}(\theta,\phi)]r^{-l-1}dV, \tag{5}$$

where the asterisk indicates a complex conjugate and the integration is performed over the source volume. Note that in Ref. [30], Eq. (15) is missing a minus sign in front of it. As can be seen, the choice of the origin affects the multipole moments; a natural choice is the center of the current-density distribution. Combining Eqs. (1) and (3), we find

$$\begin{aligned}\boldsymbol{B}(\boldsymbol{r}) = &-\mu_0\sum_{l=0}^{\infty}\sum_{m=-l}^{l}\alpha_{lm}\nabla\left(\frac{Y_{lm}(\theta,\phi)}{r^{l+1}}\right) \\ &-\mu_0\sum_{l=0}^{\infty}\sum_{m=-l}^{l}\beta_{lm}\nabla\left(Y_{lm}(\theta,\phi)r^{l}\right).\end{aligned} \tag{6}$$

If the smallest-order multipole moments $\alpha_{lm}$ are zero, the magnetic field of a coil decays rapidly with increasing distance; thus, we would like to design a self-shielded polarizing coil such that $\alpha_{lm} = 0$, for $l = 0, 1, \ldots, n$. Because $Y_{00}$ is a constant, Eq. (4) reveals that $\alpha_{00} = 0$ for every $\boldsymbol{J}(\boldsymbol{r})$. In addition, the shielding should not reduce the field amplitude at the coil center too much.

From Eq. (4), we find that for an $\boldsymbol{e}_\phi$-directional axially-symmetric current density $\boldsymbol{J}(\boldsymbol{r}) = J(r,\theta)\boldsymbol{e}_\phi$, $\alpha_{lm} = 0$, when $m \neq 0$. The other multipole moments are

$$\alpha_l = -\frac{1}{l+1}\sqrt{\frac{\pi}{2l+1}}\int_0^{\infty}\int_0^{\pi} J(r,\theta)r^{l+2}\sin\theta\frac{\partial P_l(\cos\theta)}{\partial\theta}\,d\theta\,dr \tag{7}$$

$$= \int_0^{\infty}\int_0^{\pi} J(r,\theta)K_l^{(\alpha)}(r,\theta)\,d\theta\,dr, \tag{8}$$

where we have dropped out the unnecessary index $m$, $P_l$ is the $l$:th Legendre polynomial, and $K_l^{(\alpha)}(r,\theta)$ is a kernel function for the $l$:th multipole moment. For a circular turn at $(r_0,\theta_0)$, the current density

$$\boldsymbol{J}^{(c)}(\boldsymbol{r}) = \frac{I\boldsymbol{e}_\phi}{r}\delta(r-r_0)\delta(\theta-\theta_0), \tag{9}$$

where $\delta$ is Dirac's delta function. Inserting $\boldsymbol{J}^{(c)}$ into Eq. (7) and carrying out the integrations, we get the respective multipole moments:

$$\alpha_l^{(c)} = -\frac{1}{l+1}\sqrt{\frac{\pi}{2l+1}}Ir_0^{l+1}\sin\theta_0\frac{\partial P_l(\theta)}{\partial\theta}\bigg|_{\theta=\theta_0}. \tag{10}$$

Table 1 lists the first multipole moments for a circular turn in cylindrical coordinates $(\rho,\phi,z)$.

Suppose $\alpha_i^{(0)}$, $i = 1,\ldots,n$, are the first multipole moments of a given unshielded polarizing coil. We wish to design a shielding coil

**Table 1**
The first multipole moments for a circular loop at the $z$ axis with current $I$, radius $\rho$, and axial coordinate $z$.

| $l$ | $\alpha_l^{(c)}$ |
|---|---|
| 1 | $\frac{1}{2}\sqrt{\frac{\pi}{3}}I\rho^2$ |
| 2 | $\sqrt{\frac{\pi}{5}}I\rho^2 z$ |
| 3 | $-\frac{3}{8}\sqrt{\frac{\pi}{7}}I\rho^2(\rho^2-4z^2)$ |
| 4 | $\frac{\sqrt{\pi}}{6}I\rho^2(-3\rho^2+4z^2)z$ |
| 5 | $\frac{5}{16}\sqrt{\frac{\pi}{11}}I\rho^2(\rho^4-12\rho^2z^2+8z^4)$ |

with a current density $J^{(1)}(r,\theta)\boldsymbol{e}_\phi$ that has the opposite multipole moments:

$$\alpha_i^{(1)} = \int_0^\infty \int_0^\pi J^{(1)}(r,\theta)K_i^{(\alpha)}(r,\theta)\,d\theta\,dr = -\alpha_i^{(0)}, \quad i = 1,\ldots,n. \tag{11}$$

Thus, when the coils are connected in series, the first $n$ multipole moments become zero.

One practical approach to design the shielding coil is to consider a fixed number of loops. Then, the positions and the diameters of the loops can be optimized such that the lowest multipole moments of the polarizing coil are shielded to zero.

However, here we find a solution for the unknown $J^{(1)}$ by expanding it in the basis defined by the kernel functions:

$$J^{(1)}(r,\theta) = \sum_{j=1}^{n} c_j K_j^{(\alpha)}(r,\theta). \tag{12}$$

Then,

$$\alpha_i^{(1)} = -\alpha_i^{(0)} = \sum_{j=1}^{n} c_j \int_0^\infty \int_0^\pi K_i^{(\alpha)}K_j^{(\alpha)}\,d\theta\,dr, \quad i = 1,\ldots,n \tag{13}$$

or

$$\boldsymbol{\alpha}^{(0)} = -\mathbf{K}^{(\alpha)}\boldsymbol{c}, \tag{14}$$

where $\boldsymbol{\alpha}^{(0)}$ is a vector with elements $\alpha_i^{(0)}$, the matrix $\mathbf{K}^{(\alpha)}$ contains the kernel integrals $\int\int K_i^{(\alpha)}K_j^{(\alpha)}\,d\theta\,dr$, and $\boldsymbol{c}$ is an unknown vector with elements $c_j$. A solution of Eq. (14) describes a current distribution of a shielding coil. We can constrain $J^{(1)}$ to lie on a bounded region by setting it and the kernel functions explicitly to zero elsewhere and by modifying the integration limits in Eqs. (11) and (13) to reflect the choice. As long as the functions $K_i$ are linearly independent, which is often the case, $\mathbf{K}^{(\alpha)}$ is nonsingular, meaning that there always exists a solution in the space spanned by $K_i^{(\alpha)}(r,\theta)$, $i = 1,\ldots,n$. However, care must be taken when limiting the source space. For example, Table 1 reveals that a circular turn at the positive $z$ axis with nonzero current always has a nonzero $\alpha_2$. Then again, if the space of $J^{(1)}$ is limited to the $z = 0$ plane, $\alpha_2$ is always zero.

Note that there exist infinitely many shielding coils, because any current density orthogonal to the functions $K_i^{(\alpha)}(r,\theta)$, in the sense of Eq. (11), can be added to the obtained solution without sacrificing Eq. (11). Generally, the basis functions for the current density may be chosen to be different from the functions $K_i^{(\alpha)}$. The basis functions together with the geometrical constraints define the outcome of the design process.

If we want to have a precise control of the field inside the coil, we may explore the $\beta_{lm}$ multipole moments. As with the $\alpha_{lm}$ moments, $\beta_{lm}$ moments of an axially symmetric current density distribution are zero when $m \neq 0$. The kernel functions for the $\beta_{l0}$ multipoles are

$$K_l^{(\beta)} = \frac{1}{l}\sqrt{\frac{\pi}{2l+1}}\int_0^\infty \int_0^\pi J(r,\theta)r^{-l+1}\sin\theta\frac{\partial P_l(\cos\theta)}{\partial\theta}\,d\theta\,dr. \tag{15}$$

Now, we may modify Eq. (12) and expand $J^{(1)}$ in the basis defined by both $K_l^{(\alpha)}$ and $K_l^{(\beta)}$ functions. Finally, Eq. (14) may be rewritten to include also the $\beta_{lm}$ multipole moments. With these changes, the formalism may be utilized to design self-shielded coils with a desired magnetic field profile in the interior region, *e.g.*, self-shielded gradient coils.

## 3. Methods

In the ULF-MRI test system at Aalto University, we have a cylindrical polarizing coil with $N_p = 211$ turns of 3-mm copper wire in five layers, height $h_p = 0.14$ m, and inner and outer radii $s_{in} = 0.105$ m and $s_{out} \approx 0.12$ m, respectively. The polarizing coil, with its axis in the vertical direction, is located approximately at the center of a double-layer MSR. Both layers have an inner $\mu$-metal shell and an outer aluminum shell. The height, width, and length of the innermost shielding layer are 2.76, 3.11, and 4.11 m, respectively.

The current in the polarizing coil is switched off rapidly with a dedicated circuit allowing us to reduce the polarizing field nearly linearly to zero in 1 ms. However, such a rapid decay induces significant eddy currents in conductive materials, most notably in the aluminum layers of the MSR [12,13]. These currents decay in a multi-exponential manner, the longest time constants being on the order of 1 s. When a strong polarizing field is used, the decaying eddy currents may distort the spin dynamics of a sample at the center of the room, making MRI difficult.

In our ULF-MRI test setup, we have three planar sensor modules, each having two orthogonal SQUID gradiometers, with a baseline of 8 mm and rectangular pickup loops with dimensions 13 mm × 31 mm, and one SQUID magnetometer with a square pickup loop with a side length of 27 mm. The planar sensor geometry has been optimized for MEG [31]. The sensors are situated on the curved bottom surface of a fiberglass dewar, surrounded by the polarizing coil, as illustrated in Fig. 1. The normals of the sensor modules form angles 12°, 30°, and 48° with the vertical direction. The SQUIDs with lead-wire pickup coils are shielded against the strong polarizing field in two ways [32]. Flux dams [33,34] added in series with the pickup loop and the intermediate flux transformer restrict the field originating from the pickup. 250-μm-thick and 13-mm-wide niobium plates are placed below and above the SQUID chip to provide local protection against the external field. Consequently, the sensors spontaneously recover from the prepolarization without external heating.

We adapted the method of this paper to design a shielding coil that would reduce the induced eddy currents to a tolerable level. When the coils are connected in series, the phases of the currents in them are automatically equal, making the shielding effective. We studied theoretically different axially-symmetric shielding-coil geometries that would be easy to realize: possible geometries were

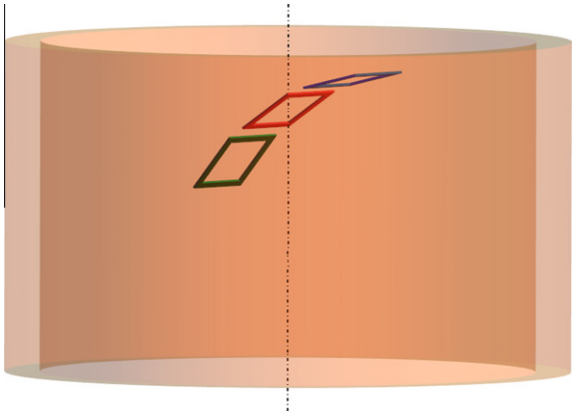

**Fig. 1.** An illustration of the sensor geometry. Shown are the cylindrical polarizing coil and the pickup loops of the three SQUID magnetometers. The dashed line marks the axis of the polarizing coil which passes through the center of a magnetometer. The normals of the magnetometers form angles 12°, 30°, and 48° with the coil axis.

a cylindrical shell, a hollow disk at the $z = 0$ plane, and a coil with multiple cylindrical shells. For practical reasons, the outer diameter of the shielding coil was limited to 0.63 m. The applied coordinate system has its origin at the center of the polarizing coil with the $z$ axis parallel to the coil axis.

We modeled the polarizing coil as a hollow cylinder with a uniform current density. Thus, the current density of the coil can be written as

$$\boldsymbol{J}_{\mathrm{p}}(\boldsymbol{r}) = J_{\mathrm{p}}(\rho, z)\boldsymbol{e}_{\phi} = \Pi_{-\frac{h_{\mathrm{p}}}{2},\frac{h_{\mathrm{p}}}{2}}(z)\Pi_{s_{\mathrm{in}},s_{\mathrm{out}}}(\rho)J_{\mathrm{p}}\boldsymbol{e}_{\phi}, \tag{16}$$

where $J_{\mathrm{p}} = N_{\mathrm{p}}I_{\mathrm{p}}/[h_{\mathrm{p}}(s_{\mathrm{out}} - s_{\mathrm{in}})]$, $I_{\mathrm{p}}$ is the current in the wire, and the boxcar function $\Pi_{a,b}(s) = 1$ when $a \leqslant s \leqslant b$, and zero otherwise. Using $\boldsymbol{J}_{\mathrm{p}}$, $\boldsymbol{\alpha}^{(0)}$ in Eq. (14) was calculated. We studied shielding coils that would null the first two or the first four $\alpha_l$ moments of the polarizing coil.

Eq. (14) was solved for the different shielding geometries. Then, the obtained surface current densities were discretized with the stream function technique to get winding patterns for sets of discrete current turns [35,36]. The number of turns in the shielding coils were matched to produce good shielding of the target multipoles when connected in series with the polarizing coil.

We compared the magnetic field of the polarizing coil with and without the shielding. The field around the coil was calculated assuming permeability of $\mu_0$. In addition, we computed the field value at the origin to check that the shielding does not reduce the polarizing field amplitude too much.

We also studied how a pair of circular coils should be positioned to shield the lowest-order multipole moments. From Table 1, it is evident that a pair of circular coils symmetric with respect to $z = 0$ could be used to shield $\alpha_1$, $\alpha_2$, …, $\alpha_4$ of the polarizing coil. With more coils, higher multipoles could also be matched, but the shielding coil would become more complex.

On the basis of the theoretical results, we constructed a single-layer cylindrical shielding coil. The winding of the coil was adjusted by inspecting signals of the SQUID sensors in the time window 20–70 ms after polarizing pulses. The aim of this tuning was to find the number of turns that would best reduce the transient magnetic fields in practice.

Finally, we measured the transient magnetic fields of the unshielded and self-shielded polarizing coils with the three SQUID magnetometers. We applied a static polarizing field for 2900 ms, after which it was switched off in 1 ms; the rise time of the field was less than 30 ms. The signal acquisition began 200 ms after the polarization, except when measuring the transient fields of the shielded polarizing coil with a small current, in which case the acquisition started 15 ms after the polarization. Before the signal acquisition, we reset the flux-locked loops of the SQUIDs.

## 4. Results

We found that a cylindrical shell with diameter $d = 0.63$ m and any length $h$ could effectively shield the multipole moments $\alpha_1$ and $\alpha_2$ of the polarizing coil. The surface current density obtained from Eq. (14) is uniform, as expected. After matching the number of turns, the coil would have 27 equally spaced turns around $z = 0$. Such a coil with $h = 0.185$ m (Fig. 2A) would reduce the polarizing field at the origin by some 5%. In Fig. 3, we show how the shielding affects the magnetic field around the coil.

To produce practical shielding against the first four multipole moments, $\alpha_1$, $\alpha_2$, …, $\alpha_4$, of the polarizing coil, a cylindrical shell with diameter $d = 0.63$ m should be at least $h = 0.4$ m long (Fig. 2B). Fig. 4 illustrates the required surface current density and the discretized winding pattern for such a coil with 27 turns. That coil would reduce the polarizing field at the origin by 4%. Fig. 5 visualizes the shielded magnetic field around the coil. Note that the stray field is significantly lower than with the 0.185-m-long shielding coil having equally spaced turns. If $h < 0.4$ m, the surface current density on the cylinder would have both positive and negative values. Then, a large number of turns would be needed, because opposing currents would produce some cancellation for the coil's dipole moment.

According to our results, a disk shield at $z = 0$ plane would shield the $\alpha_1$, $\alpha_2$, …, $\alpha_4$ multipole moments inefficiently. Such a coil would require both positive and negative currents; thus, the number of turns needed to shield the polarizing coil would be high. For our purposes, a multi-layer cylindrical shield would not produce improvements with respect to a single-layer shield. A short ($h < 0.4$ m) multi-layer shielding coil would, as a single-layer shielding coil, require currents with opposing signs to shield the $\alpha_3$ moment of the polarizing coil, leading to inefficient shielding.

Fig. 6 illustrates how a symmetrical pair of coils on the $z$ axis (see, Fig. 7) should be manufactured to shield the first four multipole moments of the polarizing coil. The figure shows the coil parameters as a function of the number of turns. When the number of turns increases, the radius of the shielding coil decreases so that its dipole moment still matches that of the polarizing coil. With our polarizing coil, this type of shielding coil resembles closely a Helmholtz pair.

Based on theoretical results and geometrical constraints, we manufactured a single-layer cylindrical shielding coil with length $h = 0.185$ m and diameter 0.63 m to shield the dipole moment of the polarizing coil. We tested the coil by varying the number of its equally spaced turns and found that the smallest transient was obtained with 28 turns. In addition, we fine-tuned the shielding by winding four new turns around the polarizing coil, in the same direction as the original ones.

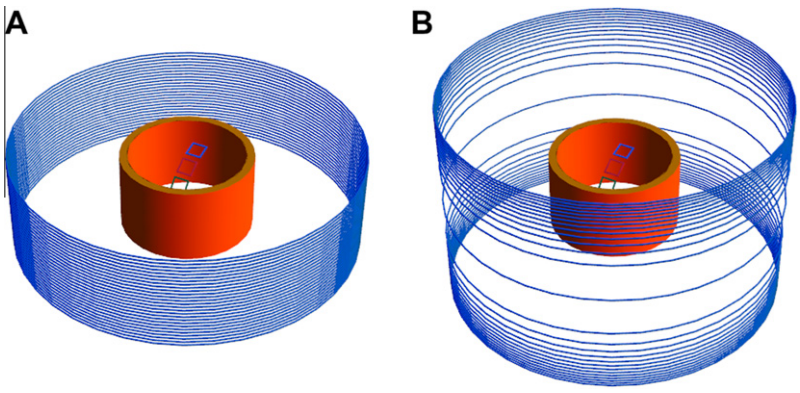


**Fig. 2.** Illustration of the polarizing (orange) and shielding (blue) coils; also shown are the pickup loops of the three SQUID magnetometers. (A) The 0.185-m-long cylindrical shielding coil with 27 equally spaced turns and diameter $d = 0.63$ m. (B) The 0.4-m-long cylindrical shielding coil with diameter $d = 0.63$ m and 27 turns positioned according to Fig. 4. (For interpretation of the references to color in this figure legend, the reader is referred to the web version of this article.)

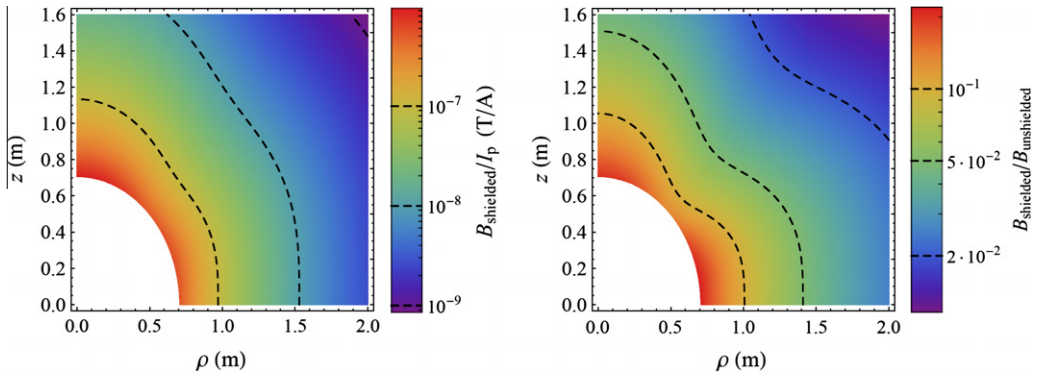


**Fig. 3.** Left: The calculated magnetic field amplitude of the polarizing coil when it is connected in series with a 0.185-m-long cylindrical shielding coil having 27 equally spaced turns and diameter $d = 0.63$ m. Current $I_p$ flows in the coils. Right: The relative amplitude between the shielded and unshielded polarizing fields using the 0.185-m-long shielding coil. For visualization, a region around the coil is plotted white. The coil geometry is illustrated in Fig. 2A.

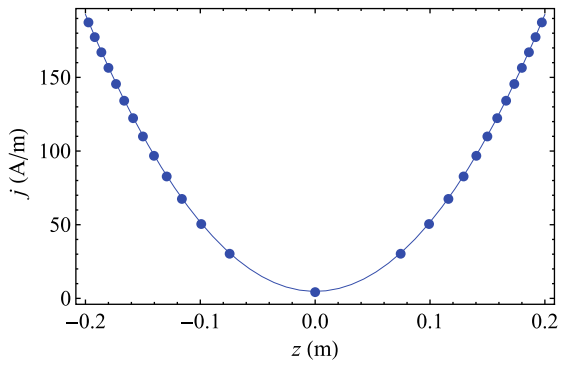


**Fig. 4.** Winding pattern for a 0.4-m-long cylindrical coil, with diameter 0.63 m, that shields against the $\alpha_1, \alpha_2, \ldots, \alpha_4$ moments of the polarizing coil. The dots mark the discrete wire positions. Also shown is the continuous surface current density $j$ obtained from Eq. (14) when a 1-A current flows in the polarizing coil.

Fig. 8 shows experimental results with and without the shielding coil. To remove high-frequency noise, the curves were moving-average filtered. When using the polarizing coil without shielding, the applied current was 600 mA, corresponding to a polarizing field $B_p = 0.61$ mT; the signal acquisition started 200 ms after the field switch-off. With the shielded polarizing coil, we measured the transient magnetic fields in two parts. The initial part from 15 to 500 ms was measured using a polarizing field $B_p = 0.43$ mT, which was achieved with a current of 440 mA. This guaranteed that all the magnetometers were working properly shortly after the field switch-off. The latter parts of the curves were obtained with a stronger polarizing field, $B_p = 7.9$ mT, achieved with a current of 8.1 A, to increase the SNR of the transient field measurement.

As can be seen, when the polarizing field is applied without shielding, the measured magnetic fields are strong and decay exponentially with long time constants. By fitting the data with a sum of two exponential functions, we found time constants 100 ms and 500 ms. By extrapolating, we found that the vertical component of the transient magnetic field at the sensor positions at $t = 0$ would have been $5–7 \times 10^{-6}\, B_p$, where $B_p$ is the vertical polarizing field at the coil center. However, this is probably an underestimate of the magnetic fields originating from the eddy currents, because the data do not reveal fields decaying with short time constants.

Fig. 8 demonstrates the benefit of using a self-shielded polarizing coil. For example, 200 ms after the polarization the magnetic field with the unshielded polarizing coil is about 50 times higher than the field achieved with the shielded coil. This result is in good agreement with the calculated magnetic fields of Fig. 3; in that figure, we see that at the distance of the walls of the MSR, the unshielded magnetic field is approximately 20–50 times higher than the shielded field.

## 5. Discussion

As can be seen from Fig. 8, even with the self-shielded polarizing coil, some decaying magnetic fields remain in our measurement environment. However, those fields decay with short

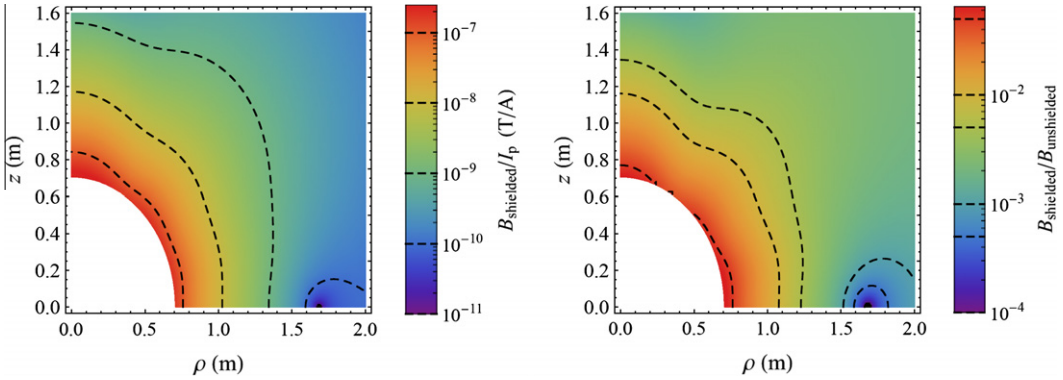


**Fig. 5.** Left: The calculated magnetic field amplitude of the polarizing coil when it is connected in series with the 0.4-m-long cylindrical shielding coil with diameter $d = 0.63$ m. The turn positions for the shielding coil are shown in Fig. 4. Current $I_p$ flows in the coils. Right: The relative amplitude between the shielded and unshielded polarizing fields using the 0.4-m-long shielding coil. For visualization, a region around the coil is plotted white. The coil geometry is visualized in Fig. 2B

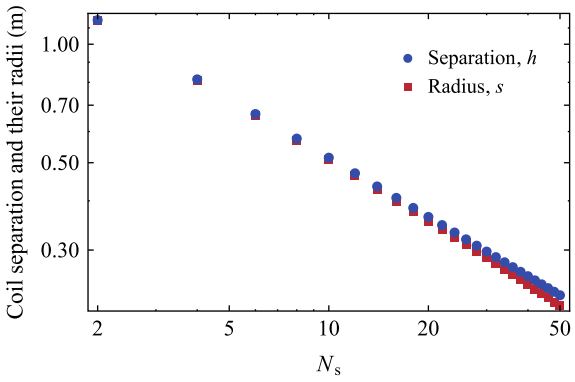


**Fig. 6.** Design parameters of a symmetric pair of coils that cancels $\alpha_1$, $\alpha_2$, ..., $\alpha_4$ moments of our polarizing coil. The horizontal axis shows the total number of turns $N_s$ in the shielding coil. The geometry of the coil is illustrated in Fig. 7.

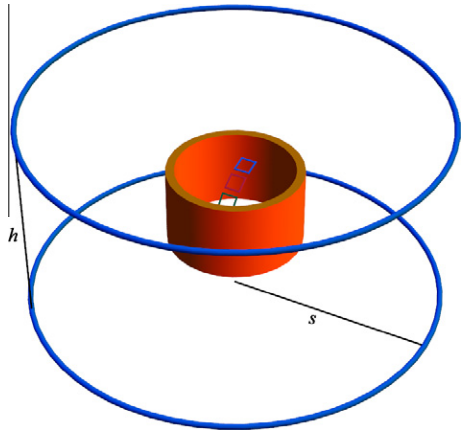


**Fig. 7.** Illustration of the polarizing coil (orange) and a shielding coil pair (blue); also shown are the pickup loops of the three SQUID magnetometers. The radius, $s$, and the separation, $h$, of the shielding coil are shown in the figure. In this figure, the geometry of the shielding coil is such that 20 turns in it would cancel out the $\alpha_1$, $\alpha_2$, ..., $\alpha_4$ moments of the polarizing coil. (For interpretation of the references to color in this figure legend, the reader is referred to the web version of this article.)

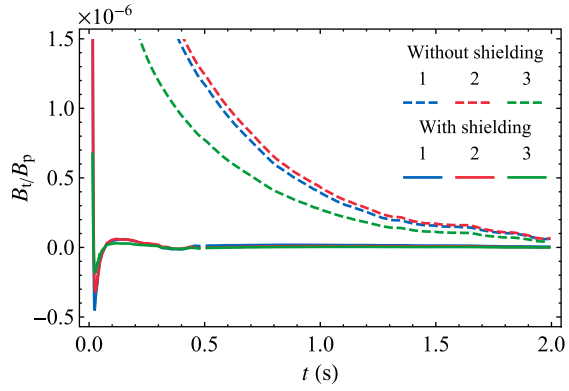


**Fig. 8.** Transient magnetic field $B_t$ measured with the three SQUID magnetometers after the polarizing field was switched off. $t$ is the time after the field switch-off and $B_p$ is the polarizing field at the center of the polarizing coil.

relaxation time constants and are not as harmful as the long-lasting fields. Because of their short time constants, we think that these fields are not generated by eddy currents circulating in the main loops of the MSR.

If high-precision shielding is needed, it may be best to fine-tune the shielding on-site by measuring the actual transient magnetic fields and adjusting the winding. Such a need may arise if the multipole moments of the coils are only known inaccurately. Depending on the precise geometry of the conductive structures nearby, nulling the lowest-order multipoles may even be suboptimal.

In our case, we found that the shielding was best when we had 28 and 215 turns in the shielding and polarizing coils, respectively; with these figures, the total dipole moment seemed to be experimentally closest to zero. This is in excellent agreement with the theoretical results obtained with 27 and 211 turns in the coils. If we allow a 1-mm error for the coil radii we used to design the shielding coil, the total dipole moment of a coil with 28 + 215 turns is zero within the assumed error margin and the theoretical and experimental results agree.

If the polarizing coil is designed before the shielding coil, the discrete number of turns in the polarizing coil may limit the best possible shielding if the geometry of the shielding coil is restricted. Optimally, the polarizing coil and the shielding should be designed together so that the number of turns can be matched to guarantee optimal multipole nulling. If the shielding coil is made adjustable, the shielding can be tuned on site.

The choice of the expansion origin affects the multipole moments of a coil. Natural choices for the origin are the center of the imaging region and the center of the MSR. If these two points are close to each other, as is probably best in order to minimize the distortions caused by the MSR, the effect of the origin seems to be small and the most practical choice should be preferred.

For simplicity, we mainly restricted our formalism to axially symmetric coils. However, with slight modifications to the notation, the method can be applied also to design coils without any symmetry. Such a need may arise, *e.g.,* when the shape of the polarizing coil is spatially constrained. In this study, we ignored the multipole expansion of the coil in the interior region, but the presented formalism gives also full control, *e.g.,* over the field homogeneity or linearity in the imaging region.

In the demonstrations with our ULF-MRI test system, the highest polarizing field was 8 mT requiring an 8-A current. Although the field can still be increased at least by a factor of 2 or 3 just by increasing the current in the coil, the coil heating limits the highest achievable field. One possibility to overcome this limit is to provide the coil with cooling. Another approach to reduce the resistive dissipation is to wind the coil from superconducting wire and to mount it inside the dewar.

## 6. Conclusion

We have introduced a method for designing self-shielded polarizing coils for ultra-low-field MRI. By requiring that the lowest-order multipole moments of a shielding coil coincide those of the polarizing coil and by connecting these coils in series with reversed currents a coil with weak stray field is obtained. The resulting self-shielded polarizing coil allows us to pulse the polarizing field without inducing significant eddy currents in the layers of the magnetically shielded room. Thus, the self-shielded design permits us to use much stronger polarizing fields than without the shielding. Noteworthily, the shielding reduces the polarizing field strength at the coil center only by a small amount, whereas the eddy currents are greatly suppressed.

The self-shielded polarizing coil design allows us to use SQUID magnetometers for signal detection; commonly, second-order axial gradiometers have been used for ULF MRI [1,2]. Typically, with second-order gradiometers the eddy-current fields generate only weak signals; still, the effect on the spin dynamics remains. In addition, even with second-order gradiometers, the eddy currents

may interfere with MEG recordings, preventing simultaneous MEG–MRI [7]. Magnetometers and planar gradiometers are convenient in hybrid MEG–MRI with whole-head coverage and a large number of sensors.

With the presented shielding technique, ULF-MRI devices can utilize stronger and spatially broader polarizing fields than could be achieved with unshielded polarizing coils. The design approach is simple and can also be applied to update existing ULF-MRI systems, as was demonstrated in this study. With the described technique, a self-shielded coil may be designed to satisfy also possible spatial limitations. We believe that essentially all ULF-MRI systems in magnetically shielded rooms will benefit from self-shielded polarizing coils.

## Acknowledgments

The research leading to these results has received funding from the European Community's Seventh Framework Programme (FP7/2007–2013) under *Grant Agreement* No. 200859 and from the Instrumentarium Science Foundation.

## References

[1] R. McDermott, S.K. Lee, B. ten Haken, A.H. Trabesinger, A. Pines, J. Clarke, Microtesla MRI with a superconducting quantum interference device, Proc. Natl. Acad. Sci. U. S. A. 101 (2004) 7857–7861.
[2] V.S. Zotev, A.N. Matlachov, P.L. Volegov, H.J. Sandin, M.A. Espy, J.C. Mosher, A.V. Urbaitis, S.G. Newman, R.H. Kraus Jr., Multi-channel SQUID system for MEG and ultra-low-field MRI, IEEE Trans. Appl. Supercond. 17 (2007) 839–842.
[3] I.M. Savukov, V.S. Zotev, P.L. Volegov, M.A. Espy, A.N. Matlashov, J.J. Gomez, R.H. Kraus Jr., MRI with an atomic magnetometer suitable for practical imaging applications, J. Magn. Reson. 199 (2009) 188–191.
[4] M. Pannetier, C. Fermon, G. Le Goff, J. Simola, E. Kerr, Femtotesla magnetic field measurement with magnetoresistive sensors, Science 304 (2004) 1648–1650.
[5] M. Pannetier-Lecoeur, C. Fermon, N. Biziere, J. Scola, A.L. Walliang, RF response of superconducting-GMR mixed sensors, application to NQR, IEEE Trans. Appl. Supercond. 17 (2007) 598–601.
[6] V.S. Zotev, A.N. Matlashov, P.L. Volegov, I.M. Savukov, M.A. Espy, J.C. Mosher, J.J. Gomez, R.H. Kraus Jr., Microtesla MRI of the human brain combined with MEG, J. Magn. Reson. 194 (2008) 115–120.
[7] P.E. Magnelind, J.J. Gomez, A.N. Matlashov, T. Owens, J.H. Sandin, P.L. Volegov, M.A. Espy, Co-registration of MEG and ULF MRI using a 7 channel low-$T_c$ SQUID system, IEEE/CSC & ESAS Eur Supercond News Forum 4 (2010).
[8] J. Clarke, M. Hatridge, M. Mößle, SQUID-detected magnetic resonance imaging in microtesla fields, Annu. Rev. Biomed. Eng. 9 (2007) 389–413.
[9] D. Cohen, Large-volume conventional magnetic shields, Rev. Phys. Appl. 5 (1970) 53–58.
[10] R. McDermott, N. Kelso, M. Mößle, M. Mück, W. Myers, B. ten Haken, H.C. Seton, A.H. Trabesinger, A. Pines, J. Clarke, SQUID-detected magnetic resonance imaging in microtesla magnetic fields, J. Low Temp. Phys. 135 (2004) 793–821.
[11] V.S. Zotev, A.N. Matlashov, P.L. Volegov, A.V. Urbaitis, M.A. Espy, R.H. Kraus Jr., SQUID-based instrumentation for ultralow-field MRI, Supercond. Sci. Technol. 20 (2007) S367–S373.
[12] P.T. Vesanen, J.O. Nieminen, J. Dabek, R.J. Ilmoniemi, Hybrid MEG–MRI: geometry and time course of magnetic fields inside a magnetically shielded room, in: S. Supek, A. Sušac (Eds.), 17th International Conference on Biomagnetism Advances in Biomagnetism – Biomag, IFMBE Proceedings, vol. 28, Springer, Berlin Heidelberg, 2010, pp. 78–81.
[13] P.T. Vesanen, J.O. Nieminen, K.C.J. Zevenhoven, J. Dabek, J. Simola, J. Sarvas, R.J. Ilmoniemi, The spatial and temporal distortion of magnetic fields applied inside a magnetically shielded room, submitted for publication.
[14] W.A. Edelstein, R.A. Hedeen, R.P. Mallozzi, S.-A. El-Hamamsy, R.A. Ackermann, T.J. Havens, Making MRI quieter, Magn. Reson. Imaging 20 (2002) 155–163.
[15] P. Mansfield, B. Chapman, Active magnetic screening of coils for static and time-dependent magnetic field generation in NMR imaging, J. Phys. E: Sci. Instrum. 19 (1986) 540–545.
[16] P.B. Roemer, S. Hickey, Self-shielded gradient coils for nuclear magnetic resonance imaging, US Patent No. 4737716.
[17] R. Turner, R.M. Bowley, Passive screening of switched magnetic field gradients, J. Phys. E: Sci. Instrum. 19 (1986) 876–879.
[18] K. Yoda, Analytical design method of self-shielded planar coils, J. Appl. Phys. 67 (1990) 4349–4353.
[19] S. Crozier, S. Dodd, K. Luescher, J. Field, D.M. Doddrell, The design of biplanar, shielded, minimum energy, or minimum power pulsed $B_0$ coils, MAGMA 3 (1995) 49–55.
[20] S. Kakugawa, N. Hino, A. Komura, M. Kitamura, H. Takeshima, T. Yatsuo, H. Tazaki, Shielding stray magnetic fields of open high field MRI magnets, IEEE Trans. Appl. Supercond. 14 (2004) 1639–1642.
[21] M. Kitamura, S. Kakugawa, K. Maki, An optimal design of coaxial coils with constraints on inner and outer multipole magnetic fields, IEEE Trans. Appl. Supercond. 14 (2004) 1862–1865.
[22] P. Jehenson, M. Westphal, N. Schuff, Analytical method for the compensation of eddy-current effects induced by pulsed magnetic field gradients in NMR systems, J. Magn. Reson. 90 (1990) 264–278.
[23] J.J. Van Vaals, A.H. Bergman, Optimization of eddy current compensation, J. Magn. Reson. 90 (1990) 52–70.
[24] C.H. Boesch, R. Gruetter, E. Martin, Temporal and spatial analysis of fields generated by eddy currents in superconducting magnets: optimization of corrections and quantitative characterization of magnet/gradient systems, Magn. Reson. Med. 20 (1991) 268–284.
[25] Y. Lai, X. Jiang, A method to reduce eddy currents within iron pole plates of a 0.3 T NdFeB MRI magnet, IEEE Trans. Appl. Supercond. 12 (2002) 737–739.
[26] D.V. Berkov, R. Kötitz, Irreversible relaxation behaviour of a general class of magnetic systems, J. Phys.: Condens. Matter 8 (1996) 1257–1266.
[27] M. Burghoff, S. Hartwig, W. Kilian, A. Vorwerk, L. Trahms, SQUID systems adapted to record nuclear magnetism in low magnetic fields, IEEE Trans. Appl. Supercond. 17 (2007) 846–849.
[28] J.D. Jackson, Classical Electrodynamics, 3rd ed., John Wiley & Sons, New York, 1999.
[29] J. Bronzan, The magnetic scalar potential, Am. J. Phys. 39 (1971) 1357–1359.
[30] S. Taulu, M. Kajola, Presentation of electromagnetic multichannel data: the signal space separation method, J. Appl. Phys. 97 (2005) 124905.
[31] A.I. Ahonen, M.S. Hämäläinen, R.J. Ilmoniemi, M.J. Kajola, J.E.T. Knuutila, J.T. Simola, V.A. Vilkman, Sampling theory for neuromagnetic detector arrays, IEEE Trans. Biomed. Eng. 40 (1993) 859–869.
[32] J. Luomahaara, P.T. Vesanen, J. Penttilä, J.O. Nieminen, J. Dabek, J. Simola, M. Kiviranta, L. Grönberg, C.J. Zevenhoven, R.J. Ilmoniemi, J. Hassel, All-planar SQUIDs and pickup coils for combined MEG and MRI, Supercond. Sci. Technol. 24 (2011) 075020.
[33] R.H. Koch, J.Z. Sun, V. Foglietta, W.J. Gallagher, Flux dam, a method to reduce extra low frequency noise when a superconducting magnetometer is exposed to a magnetic field, Appl. Phys. Lett. 67 (1995) 859–862.
[34] C. Hilbert, J. Clarke, T. Sleator, E.L. Hahn, Nuclear quadrupole resonance detected at 30 MHz with a dc superconducting quantum interference device, Appl. Phys. Lett. 47 (1985) 637–639.
[35] R. Turner, A target field approach to optimal coil design, J. Phys. D: Appl. Phys. 19 (1986) L147–L151.
[36] G.N. Peeren, Stream function approach for determining optimal surface currents, J. Comput. Phys. 191 (2003) 305–321.